



## NRC Publications Archive Archives des publications du CNRC

### **Microwave synthesis of $\text{Li}_{1.025}\text{Mn}_{1.975}\text{O}_4$ and $\text{Li}_{1+x}\text{Mn}_{2-x}\text{O}_4\text{-yF}_y$ ( $x=0.05, 0.15$ ; $y=0.05, 0.1$ )**

Whitfield, Pamela; Davidson, Isobel

This publication could be one of several versions: author's original, accepted manuscript or the publisher's version. / La version de cette publication peut être l'une des suivantes : la version prépublication de l'auteur, la version acceptée du manuscrit ou la version de l'éditeur.

For the publisher's version, please access the DOI link below. / Pour consulter la version de l'éditeur, utilisez le lien DOI ci-dessous.

#### **Publisher's version / Version de l'éditeur:**

<https://doi.org/10.1149/1.1394089>

*Journal of the Electrochemical Society*, 147, December 12, pp. 4476-4484, 2000

#### **NRC Publications Record / Notice d'Archives des publications de CNRC:**

<https://nrc-publications.canada.ca/eng/view/object/?id=9b231837-a2e8-4c8e-a744-834ad78528b5>

<https://publications-cnrc.canada.ca/fra/voir/objet/?id=9b231837-a2e8-4c8e-a744-834ad78528b5>

Access and use of this website and the material on it are subject to the Terms and Conditions set forth at

<https://nrc-publications.canada.ca/eng/copyright>

READ THESE TERMS AND CONDITIONS CAREFULLY BEFORE USING THIS WEBSITE.

L'accès à ce site Web et l'utilisation de son contenu sont assujettis aux conditions présentées dans le site

<https://publications-cnrc.canada.ca/fra/droits>

LISEZ CES CONDITIONS ATTENTIVEMENT AVANT D'UTILISER CE SITE WEB.

#### **Questions?** Contact the NRC Publications Archive team at

PublicationsArchive-ArchivesPublications@nrc-cnrc.gc.ca. If you wish to email the authors directly, please see the first page of the publication for their contact information.

**Vous avez des questions?** Nous pouvons vous aider. Pour communiquer directement avec un auteur, consultez la première page de la revue dans laquelle son article a été publié afin de trouver ses coordonnées. Si vous n'arrivez pas à les repérer, communiquez avec nous à PublicationsArchive-ArchivesPublications@nrc-cnrc.gc.ca.



# Microwave Synthesis of $\text{Li}_{1.025}\text{Mn}_{1.975}\text{O}_4$ and $\text{Li}_{1+x}\text{Mn}_{2-x}\text{O}_{4-y}\text{F}_y$ ( $x = 0.05, 0.15$ ; $y = 0.05, 0.1$ )

P. S. Whitfield\*<sup>z</sup> and I. J. Davidson\*

Institute for Chemical Process and Environmental Technology, National Research Council of Canada, Ottawa, Ontario  
K1A 0R6, Canada

The use of microwave irradiation is already established in sample preparation for analytical work [P. J. Walter, S. Chalk, and H. M. Kingston, in *Microwave-Enhanced Chemistry, Fundamentals, Sample Preparation and Application*, p. 55, American Chemical Society, Washington, DC (1997).] and in solution synthesis of organic compounds (G. Majetich and K. Wheless, *ibid.*, p. 455). The use of microwaves for solid-state synthesis is a fairly recent development but promises advantages in speed and energy efficiency. This paper presents results from a feasibility study into microwave synthesis of some electrochemically active spinel stoichiometries using an unmodified domestic microwave oven. Although much work has been reported about these materials, they are still the subject of intensive interest as potential cathodes in lithium-ion batteries, a cheap and less toxic alternative to  $\text{LiCoO}_2$ . The synthesis of  $\text{Li}_{1.025}\text{Mn}_{1.975}\text{O}_4$  was seen to be greatly accelerated by microwave heating, even at low powers. The addition of fluorine during syntheses using high power had a profound effect on the reaction rate and resultant particle shape and size. Samples produced using low power from  $\gamma\text{-MnOOH}$  showed unusual needle-like morphologies reminiscent of a chimie-douce process.  
© 2000 The Electrochemical Society. S0013-4651(00)07-029-4. All rights reserved.

Manuscript submitted July 8, 2000; revised manuscript received August 10, 2000.

Rechargeable lithium-ion batteries are becoming increasingly important as power sources for a multitude of portable consumer electronics. Currently the material of choice for the cathode material is  $\text{LiCoO}_2$ , which although having good capacity and rechargeability, suffers from the high cost and environmental toxicity of cobalt. Consequently, much effort has been put into developing alternatives. At present, the materials most likely to succeed in future commercial applications are  $\text{LiNiO}_2$ ,  $\text{LiMn}_2\text{O}_4$ ,  $\text{LiMnO}_2$ , and related substituted systems.<sup>1</sup> Manganese-based compounds are particularly attractive due to the low cost and toxicity of manganese, so a wide range of compounds of that element has been studied.<sup>2</sup>

$\text{LiMn}_2\text{O}_4$  spinel in particular came to prominence in the early 1980s after it was demonstrated that lithium ions could be reversibly intercalated into  $\text{LiMn}_2\text{O}_4$ .<sup>3,4</sup> The material exhibits a two-stage charge/discharge at 3 and 4 V vs. Li, yielding a theoretical capacity of 296 mAh/g. However, it suffered from a number of practical problems, many of which have been overcome in the intervening years. The most troubling was the spinel's lack of long-term cyclability, shown by a marked fade in discharge capacity with cycle number.<sup>2</sup> This was attributed to a number of factors, including manganese dissolution,<sup>5</sup> electrolyte decomposition,<sup>5</sup> and microstructural fatigue brought about by a Jahn-Teller induced cubic-tetragonal transition.<sup>2</sup> Limiting the cycling to the 4 V plateau reduced but did not eliminate this structural distortion, as well as reducing the available theoretical capacity to 148 mAh/g. Substitution of some of the manganese for another element, *e.g.*, excess Li, keeps the manganese oxidation state above 3.5 during cycling over the 4 V plateau, thus eliminating the Jahn-Teller distortion on discharge. This, together with an improved understanding of materials synthesis and processing,<sup>6,7</sup> has led to the achievement of good room-temperature cyclability with substituted spinel. However, its poor cyclability at elevated temperatures typically found in laptop computers, electric vehicles, etc., is an obstacle to its widespread introduction as a commercial cathode material. This mode of failure has been associated with accelerated manganese dissolution and formation of a protonated  $\lambda\text{-MnO}_2$  phase,<sup>8</sup> and efforts to combat the problem have resorted to more exotic techniques than simple cation substitution.

Fluorination as a means to change the structure and electronic properties of oxides became an established technique in the field of high-temperature cuprate superconductors.<sup>9</sup> Fluorine's ability to stabilize metastable structures made it a natural substituent in the quest

for improved high-temperature storage and cycling of the lithium manganese spinels.<sup>10-12</sup>

An alternative approach is the use of a barrier layer on the spinel particles to prevent contact with the nonaqueous electrolyte.<sup>13</sup> To date, much progress has been made, but further improvements in the elevated temperature performance of spinel are still required.

Analytical and organic chemists have used microwave irradiation for some time and have established that dissolution and reaction rates can be significantly enhanced. The absorption of microwaves by a liquid, particularly water, is an everyday experience, and it is not surprising that laboratory applications of this effect were developed. However, the absorption of microwaves by solids and subsequent heating is not as intuitively obvious, the first systematic study of such effects on inorganic minerals and compounds being carried out in the mid-1980s.<sup>14</sup> The effect of microwaves varies greatly from material to material. As may be seen in Table 1, some materials such as  $\text{SiO}_2$  show little or no heating, whereas others show dramatic temperature increases in a very short period of time. Microwave heating in solids is usually caused by dielectric and/or resistive losses within the material. Interest in the technique stems partly from the increased efficiency of processing. Magnetrons (the most common microwave source) have an efficiency of only 60%, but reactions can be accelerated to such an extent that substantial energy savings could be accrued.

Sintering of certain ceramic materials using microwave irradiation has been found to achieve beneficial results in terms of particle size, sintering temperature and firing time,<sup>15</sup> although the use of microwave irradiation in solid-state synthesis has been somewhat limited. Most work has concentrated on reactions that include reactants that absorb microwaves at room temperature. A notable exam-

**Table I. Effect of microwave heating on 5 g of some reagent-grade materials.**

Material	Temp (°C)	Time (min)	Material	Temp (°C)	Time (min)
C (amorph) <1 $\mu\text{m}$	1283	1	CuO	1012	6.25
C (graphite) <1 $\mu\text{m}$	1073	1.75	$\text{Co}_2\text{O}_3$	1290	3
C (graphite) 200 mesh	780	6	$\beta\text{-MnO}_2$	1287	6
$\text{SiO}_2$	79	7	NiO	1305	6.25

\* Electrochemical Society Active Member.

<sup>z</sup> E-mail: pamela.whitfield@nrc.ca

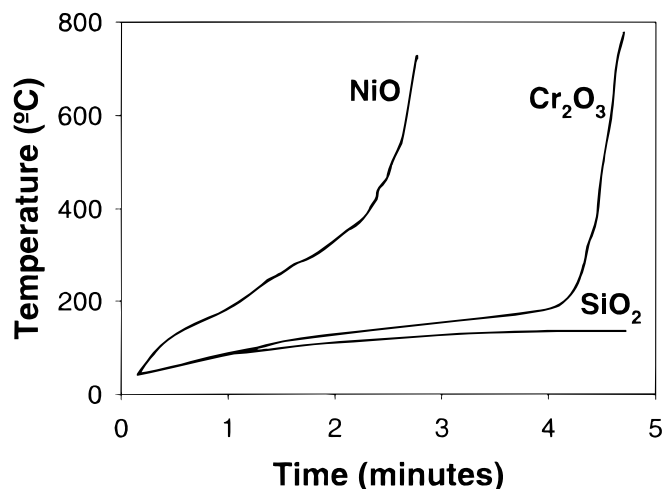


**Figure 1.** Temperature with time for NiO, Cr<sub>2</sub>O<sub>3</sub>, and SiO<sub>2</sub> irradiated with microwaves at 2.45 GHz using a power of 800 W.

ple of this is the synthesis of cuprate superconductors, in which the CuO reactant absorbs heats rapidly.<sup>16,17</sup> Recently however, an increasing number of papers have appeared in which separate susceptor materials (usually graphite) are used to heat reactant mixtures which themselves do not absorb microwaves, producing materials such as titanates.<sup>18</sup>

There is still controversy over the existence of a “microwave effect.” Numerous papers cite reduced reaction/sintering temperatures,<sup>19,20</sup> often attributed to a lowering of the reaction’s activation energy. Some disagreements resulted from these assertions,<sup>21,22</sup> the bases of which were often the practical difficulties of measuring temperatures in a microwave cavity. However, a recent theoretical treatment of the problem has concluded that such an effect exists, relating to increased mass transport.<sup>23</sup>

Microwave heating of solid materials may present a unique phenomenon known as “thermal runaway,” which has no counterpart in conventional heating. The origin of this effect is the variation of the loss tangent (*i.e.*, efficiency of microwave absorption) with temperature. In some materials this increases sharply with temperature (see Fig. 1), leading to a positive feedback loop. This may cause uncontrolled heating and melting within a sample, often with deleterious results for the material’s properties. Where this is a problem for a particular material very careful control of the sample temperature must be maintained.

Given the problems presented by the possibility of thermal runaway, it is unfortunate that one of the main difficulties encountered when carrying out microwave syntheses is temperature measurement and control. The use of thermocouples is not straightforward and requires careful design and grounding to avoid inducing large voltages through interaction with the intense electromagnetic field. Infrared pyrometry can avoid many of these problems but suffers from the limitations of measuring only the surface temperature.<sup>24</sup> Studies have shown that the surface temperature can be considerably less than that of the bulk.<sup>24</sup>

Little has appeared in the literature regarding microwave synthesis of lithium battery cathode materials. The first were two papers on the synthesis and electrochemical properties of microwave-synthesized LiCoO<sub>2</sub>.<sup>25,26</sup> The synthesis work was carried out in a custom-built “single mode” (*i.e.*, single wavelength) system that is quite different from the multimode system (*i.e.*, a range of wavelengths) used in this work.

Of the manganese-based cathode materials, LiMn<sub>2</sub>O<sub>4</sub> should be the easiest to produce as oxidation is less of a problem than with other materials, where close control of the manganese oxidation state is required. A patent was issued in 1998 regarding the microwave synthesis of LiMn<sub>2</sub>O<sub>4</sub>,<sup>27</sup> although this work to date has not been followed up by publication in a journal. The X-ray diffraction (XRD)

pattern presented in the patent suggests that this material was not very pure with significant Li<sub>2</sub>MnO<sub>3</sub> content. Microwave synthesis of pure LiMn<sub>2</sub>O<sub>4</sub> is claimed by Rao *et al.*, although no results are presented.<sup>28</sup> It is stated that using LiI as a starting material resulted in the formation of an iodine shroud, facilitating the production of pure material. This is probably correct, although the use of elemental iodine vapor limits the use of the method to small-scale synthesis and requires the use of efficient fume extraction due to safety concerns.

Very recently Yan *et al.* have followed up their work on LiCoO<sub>2</sub> with a paper describing microwave synthesis of stoichiometric LiMn<sub>2</sub>O<sub>4</sub>.<sup>29</sup> Using LiOH·H<sub>2</sub>O and MnO<sub>2</sub> (CMD), they produced material with the same particle shape and shape (10-40 μm) as the starting CMD. Temperature measurements were taken using an infrared pyrometer, and the optimum temperature range for synthesis was determined as 700-750°C. As mentioned previously infrared pyrometry can underestimate the bulk temperature, and accurate measurements require that the emissivity of the material over the entire temperature range be known.<sup>24</sup> However, this is a minor criticism as temperature measurement in a microwave cavity is not straightforward; indeed, in this work it was felt that the necessary modifications to the oven were not practical. Consequently, temperature measurements for the current syntheses will have to await the acquisition of a specialized system.

The initial discharge of their material was 120 mAh/g cycling between 3.5 and 4.5 V vs. lithium metal. Unfortunately, they did not present results on extended cycling vs. lithium but did demonstrate that the material performed reasonably well in a lithium-ion cell with a graphite anode over 300 cycles.

Strangely, no one to date has reported the synthesis of lithium-rich material, *i.e.*, Li<sub>1+x</sub>Mn<sub>2-x</sub>O<sub>4</sub> with  $x > 0$ , as this material has more useful electrochemical characteristics for use in a cathode. A possible reason for this is that the presence of excess Li makes the formation of unwanted Li<sub>2</sub>MnO<sub>3</sub> more likely, making phase pure material more difficult to obtain.

Presented in this paper are results from work studying the feasibility of using microwave irradiation as a means of producing useful electrode materials. The synthesis and physical characterization of lithium-rich and fluorinated spinels are described. Details of the structural and electrochemical characterization of these materials will appear in a future paper.

## Experimental

Experiments were carried out using a metal-lined domestic 800 W microwave oven. To facilitate the reaction of materials which do not absorb microwaves, a dual crucible system was devised using a secondary susceptor. A schematic diagram of the crucible system is shown in Fig. 2.

Unlike most of the papers in the literature,<sup>18,30</sup> CuO was chosen as the susceptor as opposed to graphite. This has a number of advantages over the more commonly used graphite. CuO partially sinters, producing a “mold” for the inner crucible to be placed in. The CuO is not consumed during the heating, unlike graphite when heated in air, which is accompanied by the risk of CO production. The disadvantages of CuO vs. graphite are that the heating rate and achievable temperature are not as high (see Table I), but the relevance of these facts depends on the desired reaction conditions.

Reactants used in the work were Mn<sub>2</sub>O<sub>3</sub> (Aldrich), β-MnO<sub>2</sub> (Aldrich), γ-MnOOH (Chemicals), LiOH·H<sub>2</sub>O (Anachemica), and LiF (Aldrich).

To date all published data on microwave syntheses of LiMn<sub>2</sub>O<sub>4</sub> have used MnO<sub>2</sub> as the Mn source because of its favorable microwave absorption characteristics. The initial work in this study used β-MnO<sub>2</sub> for the same reason.

The stoichiometries studied were chosen to have a manganese oxidation state above +3.5 (+3.53 for Li<sub>1.025</sub>Mn<sub>1.975</sub>O<sub>4</sub>, +3.54 for Li<sub>1.05</sub>Mn<sub>1.95</sub>O<sub>3.95</sub>F<sub>0.05</sub>, and +3.65 for Li<sub>1.15</sub>Mn<sub>1.85</sub>O<sub>3.9</sub>F<sub>0.1</sub>). These values correspond to theoretical capacities over the 4 V plateau of 139, 136, and 104 mAh/g, respectively.

Samples were prepared by mixing/grinding reagents of the required stoichiometry in a pestle and mortar with an acetone/ethanol mixture. This was repeated, and once dry, the mixture was placed into a small zirconia crucible. This crucible was then positioned within the larger quartz crucible in the arrangement seen in Fig. 2. The porcelain lid served the dual purposes of reducing heat loss from the sample surface and reducing air circulation within the zirconia crucible. The whole assembly was finally placed onto a firebrick on the microwave turntable. During processing the crucible was "off-center" in the microwave oven to minimize the formation of hot-spots due to standing waves in the microwave field within the cavity.

The high-temperature materials were synthesized in a one-step process. When using  $\beta$ - $\text{MnO}_2$ , power was applied for 25 min. Syntheses with  $\text{Mn}_2\text{O}_3$  and  $\gamma$ - $\text{MnOOH}$  used a simulated ramp-soak procedure, where the applied power was reduced after 9.5 min and 9 min with a total of 39.5 and 39 min for unfluorinated and fluorinated materials, respectively. The heating rate of the materials was so rapid that such a small change in the initial heating did make a noticeable difference to the final product.

The low-temperature materials were heated with a constant low power in 30 min stages with intermediate grindings. Unfluorinated and fluorinated materials were heated until phase pure, which were 3 and 2 h, respectively, for the two types of material.

An attempt was made to roughly ascertain the temperatures achieved during high-power application. The anatase-rutile phase transition was used to determine whether the microwave crucible setup in Fig. 2 reached the temperature of this transition,  $\sim 900^\circ\text{C}$ . Using high power the rutile phase could be identified by XRD with 15 min firing at full power. This approach is complicated by a reported  $100^\circ\text{C}$  reduction in the phase transformation temperature with microwave heating.<sup>31</sup> The same paper also describes the marked acceleration of this normally sluggish phase transition with microwave compared to conventional heating. Together with the glowing  $\text{CuO}$  visible in the crucible, this would suggest a temperature in the range  $800$ – $950^\circ\text{C}$ , depending on whether the accelerated rutile formation is the result of a "microwave effect" or highly elevated temperatures.

Powder X-ray data were obtained using  $\text{Cu K}\alpha$  radiation with a Scintag XDS-2000 system with a diffracted beam graphite monochromator. Preliminary refinements of lattice parameters, and simulations of cation mixing were performed using a beta version of Powder Cell 2.0.<sup>32</sup> Lattice parameters were refined and preliminary

structure analysis performed using the General Structure Analysis System package.<sup>33</sup>

Fourier transform infrared (FTIR) spectroscopy was performed on samples using a MIDAC M1200-SP3 spectrometer. The data was collected from conventional pressed KBr disks in the range  $400$ – $4000\text{ cm}^{-1}$ . Particle size analysis was carried out using a Horiba LA-920 laser scattering particle size analyzer. Analyses were done both with and without *in situ* sonication in 0.1% sodium pyrophosphate solution. The data was analyzed assuming a refractive index of 1.19. Surface area analysis data were collected using a Micromeritics ASAP 2000 system with krypton gas. Differential scanning calorimetry (DSC) was carried out using a DuPont model 2910 calorimeter. The data were collected between room temperature and  $200^\circ\text{C}$  using a ramp rate of  $5^\circ\text{C}/\text{min}$ .

Analysis for lithium and manganese content were carried out using a Varian SpectraAA 800 spectrometer. Lithium was determined by emission and manganese by absorption for optimum sensitivity. Oxygen content was derived by difference. Scanning electron microscopy (SEM) analysis was performed with a JOEL JSM 5300 scanning electron microscope with an accelerating voltage of 20 kV. The powder samples were sonicated in isopropanol for approximately 10 min. A sample of the suspension was placed onto a glass slide cover and gold-coated prior to examination.

## Results and Discussion

**High-temperature synthesis.**—Synthesis of  $\text{Li}_{1.025}\text{Mn}_{1.975}\text{O}_4$  using  $\text{MnO}_2$  and  $\text{LiOH}\cdot\text{H}_2\text{O}$  proceeded very rapidly, as shown in Fig. 3. Unfortunately,  $\text{Li}_2\text{MnO}_3$  and/or  $\text{Mn}_3\text{O}_4$  were always present as minor phases, which were never completely eliminated. Their presence suggested that high-temperatures were generated during the process, as these are expected high temperature decomposition products of the spinel.<sup>34</sup> The formation of crystalline  $\text{LiMnO}_2$  early in the reaction supports this hypothesis. The typical *a* lattice parameter of the spinel material obtained was  $8.23\text{ \AA}$ . Although  $\text{Li}_2\text{MnO}_3$  as marked in Fig. 3 was barely visible after 25 min, the fraction of this phase increased dramatically with further heating.

The particles obtained from this processing were relatively large, which was unsurprising given the particle size of the source  $\beta$ - $\text{MnO}_2$  ( $-60$  to  $+230$  mesh). SEM (Fig. 4) showed many of the particles to be heavily fissured, probably due to extreme stresses during the rapid heating.

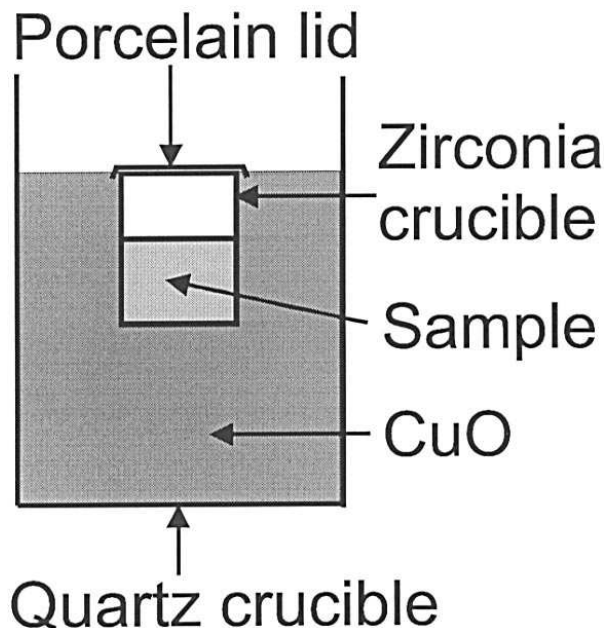


Figure 2. Crucible arrangement for microwave powder synthesis.

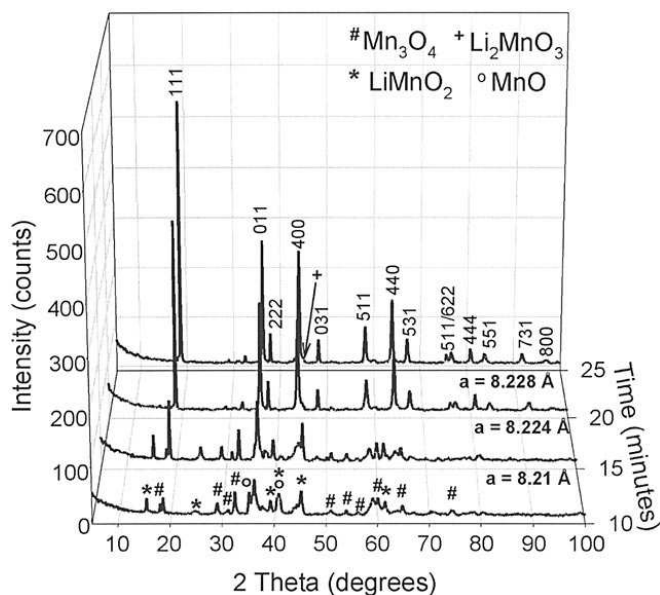
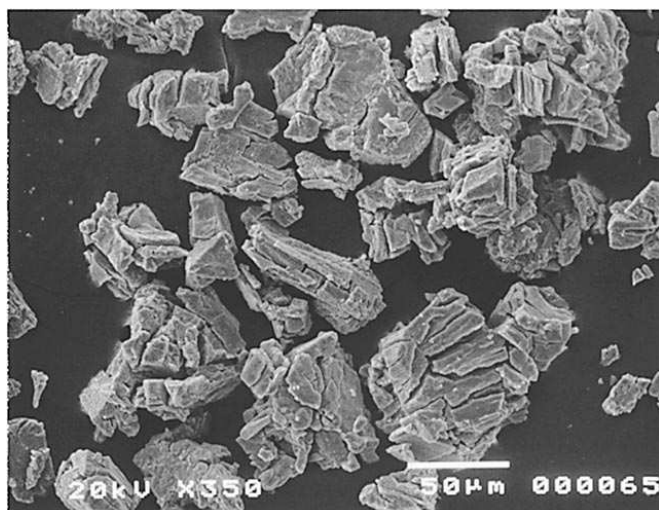


Figure 3. Evolution of X-ray powder diffraction with microwave processing time of  $\beta$ - $\text{MnO}_2$  and  $\text{LiOH}\cdot\text{H}_2\text{O}$ .



**Figure 4.** SEM micrograph of  $\text{Li}_{1.025}\text{Mn}_{1.975}\text{O}_4$  synthesized using  $\beta\text{-MnO}_2$  and  $\text{LiOH}\cdot\text{H}_2\text{O}$ .

Given that the material obtained using  $\beta\text{-MnO}_2$  had significant amounts of parasitic phases present, and the problems encountered with overheating, efforts shifted to other Mn sources. Neither  $\text{Mn}_2\text{O}_3$  nor  $\gamma\text{-MnOOH}$  absorb microwaves to any significant degree, therefore, the dual-crucible arrangement was crucial to the syntheses. Initial efforts concentrated on duplicating the high-temperature  $\beta\text{-MnO}_2$  synthesis.

Figure 5 shows the X-ray powder diffraction patterns for  $\text{Li}_{1.025}\text{Mn}_{1.975}\text{O}_4$  synthesized in 39 min from  $\text{Mn}_2\text{O}_3$  and  $\gamma\text{-MnOOH}$ , and  $\text{Li}_{1.05}\text{Mn}_{1.95}\text{O}_{3.95}\text{F}_{0.05}$  synthesized from  $\text{Mn}_2\text{O}_3$  and  $\text{LiF}$  in the same time. The materials exhibited marked differences in the relative 111, 311, and 400 intensities. By inspection, this would likely correspond to differences in cation ordering, particularly the presence of Mn on the Li site. This is supported by preliminary refinements in the cubic  $Fd\bar{3}m$  cell, which suggest Mn fractions of ~13, 7, and 6% on the Li sites in  $\text{Li}_{1.025}\text{Mn}_{1.975}\text{O}_4(\text{Mn}_2\text{O}_3)$ ,  $\text{Li}_{1.05}\text{Mn}_{1.95}\text{O}_{3.95}\text{F}_{0.05}$ , and  $\text{Li}_{1.025}\text{Mn}_{1.975}\text{O}_4(\gamma\text{-MnOOH})$ , respectively. The addition of a small quantity of fluorine appears to reduce cation mixing, and the data is

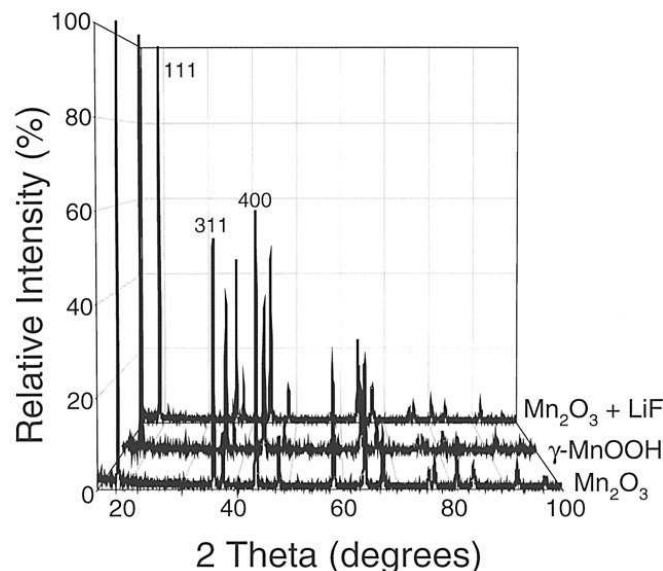


**Figure 5.** Normalized XRD patterns of  $\text{Li}_{1.025}\text{Mn}_{1.975}\text{O}_4$  synthesized at high temperature from  $\text{LiOH}\cdot\text{H}_2\text{O}$ ,  $\text{Mn}_2\text{O}_3$ , and  $\gamma\text{-MnOOH}$ , and  $\text{Li}_{1.05}\text{Mn}_{1.95}\text{O}_{3.95}\text{F}_{0.05}$  synthesized with  $\text{LiOH}\cdot\text{H}_2\text{O}$ ,  $\text{Mn}_2\text{O}_3$ , and  $\text{LiF}$ .

**Table II.** Cubic  $a$  lattice parameters for the high-temperature synthesized materials.

Material	Lattice parameter $a$ (Å)
$\text{Li}_{1.025}\text{Mn}_{1.975}\text{O}_4\text{-Mn}_2\text{O}_3$	8.23793(19)
$\text{Li}_{1.025}\text{Mn}_{1.975}\text{O}_4\text{-}\gamma\text{-MnOOH}$	8.24949(32)
$\text{Li}_{1.05}\text{Mn}_{1.95}\text{O}_{3.95}\text{F}_{0.05}$	8.24243(24)

suggestive of a more crystalline material, *i.e.*, a smaller full width at half maximum (fwhm) in this case.

The refined lattice parameters of the materials are seen in Table II. Each of the lattice parameters was larger than one would expect given the materials' nominal stoichiometries. This was most pronounced for  $\text{Li}_{1.025}\text{Mn}_{1.975}\text{O}_4$  synthesized with  $\gamma\text{-MnOOH}$ . This suggests quenching behavior during cooling,<sup>34,35</sup> although the presence of unmodeled secondary phases such as  $\text{Li}_2\text{MnO}_3$  distorting major peak profiles in GSAS full pattern fitting could contribute toward a small shift in refined values. All of the samples when analyzed by atomic absorption spectroscopy and Auger electron spectroscopy (AAS/AES) yielded nominal stoichiometries within the errors of the technique.

When one looks at the SEM pictures for the unfluorinated materials, as seen in Fig. 6a and b, there is a striking difference between the particle morphologies. Considering that  $\gamma\text{-MnOOH}$  is known to decompose to  $\beta\text{-MnO}_2$  in air at  $300^\circ\text{C}$ <sup>36</sup> this is not too surprising. The higher temperatures attained due to improved microwave absorption by the sample would lead to enhanced grain growth. This would also produce more pronounced quenching on cooling, thus leading to the larger  $a$  lattice parameter observed in the X-ray data.<sup>34,35</sup>

The SEM of the fluorinated material in Fig. 6c shows larger and more well defined crystallites than Fig. 6a. Halide salts are known to be effective mineralizing agents and are often used as a flux in crystal growth.<sup>37</sup> It is likely that the small quantity of  $\text{LiF}$  could act in a similar fashion. This raises the question of whether the fluoride ions actively enter the spinel crystal lattice or remain on the crystallite surfaces as a simple fluoride salt. Unfortunately, oxygen and fluorine have very similar X-ray form factors and neutron scattering lengths;<sup>38</sup> therefore, it is impossible to answer this definitively with conventional diffraction techniques. Techniques such as X-ray absorption fine structure (XAFS) and anomalous dispersive diffraction could separate them but are beyond the scope of this initial investigation.

Table III shows the particle sizes of the samples shown in Fig. 6 and the manganese sources. Figure 7 shows the corresponding volume frequency of the particle size distributions. This data agrees well with the observed differences in particle size by SEM, both the addition of fluorine and use of  $\gamma\text{-MnOOH}$  leading to significantly larger particle sizes. The mean and modal particle sizes of the fluorinated material were significantly different due to the bimodal nature of the distribution. This leads to the possibility of using fluorine as a method for controlling morphology and particle size as well as electrochemical and structural properties.

The high-temperature materials exhibited an infrared spectrum as shown in Fig. 8, with two strong absorption bands at 515 and  $614\text{ cm}^{-1}$ . These agree well with literature values for  $\text{LiMn}_2\text{O}_4$ .<sup>39,40</sup>

The cooling rate of the crucibles could not be controlled in the microwave oven, the rate being determined by their thermal mass and temperature. Typically an experiment cooled sufficiently after 20-25 min that it could be removed from the oven. With this apparatus the only way to control the initial cooling rate was varying the crucible temperature. Therefore materials synthesized at a lower temperature would be less likely to exhibit characteristics typical of quenching, *i.e.*, large  $a$  lattice parameter together with significant cation mixing.

*Low-temperature synthesis.*—Each of the low-temperature synthesized materials exhibited a typical spinel-type XRD pattern as

demonstrated in Fig. 9. In each case the 111/311/400 cubic reflections did not show obvious gross cation mixing. Preliminary refinements showed that the patterns fit best to the orthorhombic  $Fddd$

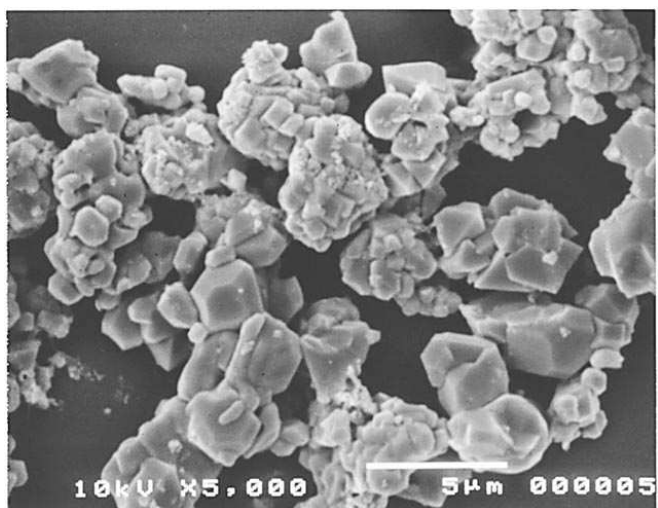
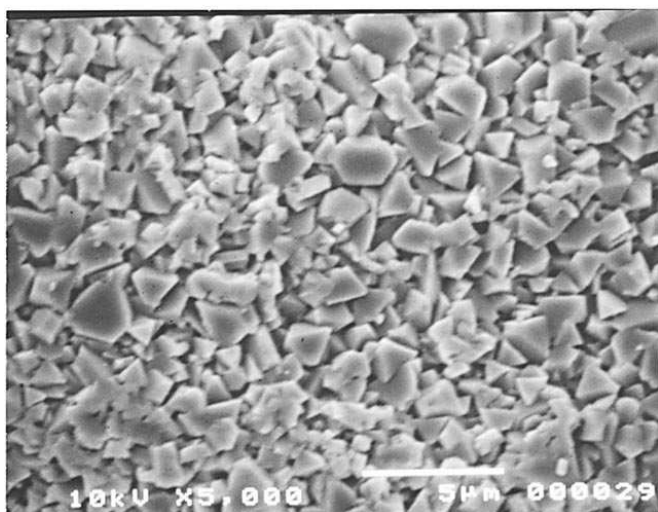
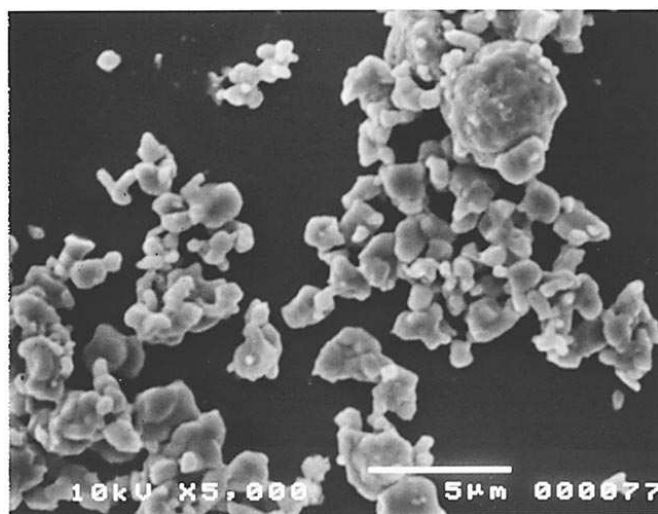


**Figure 6.** SEM micrographs of (a, top)  $\text{Li}_{1.025}\text{Mn}_{1.975}\text{O}_4$  synthesized from  $\text{LiOH}\cdot\text{H}_2\text{O} + \text{Mn}_2\text{O}_3$ , (b, center)  $\text{Li}_{1.025}\text{Mn}_{1.975}\text{O}_4$  synthesized from  $\text{LiOH}\cdot\text{H}_2\text{O} + \gamma\text{-MnOOH}$ , and (c, bottom)  $\text{Li}_{1.05}\text{Mn}_{1.95}\text{O}_{3.95}\text{F}_{0.05}$  synthesized from  $\text{Mn}_2\text{O}_3 + \text{LiOH}\cdot\text{H}_2\text{O} + \text{LiF}$ .

**Table III.** Particle sizes of the high-temperature synthesized materials together with the Mn reactants.

Material	Mean particle size volume distribution ( $\mu\text{m}$ )	Modal particle size volume distribution ( $\mu\text{m}$ )
Aldrich $\text{Mn}_2\text{O}_3$	3.0	3.2
Chemicals $\gamma\text{-MnOOH}$	0.9	0.5
$\text{Li}_{1.025}\text{Mn}_{1.975}\text{O}_4$ ( $\text{Mn}_2\text{O}_3$ )	6.0	6.3
$\text{Li}_{1.025}\text{Mn}_{1.975}\text{O}_4$ ( $\gamma\text{-MnOOH}$ )	20.6	21.3
$\text{Li}_{1.05}\text{Mn}_{1.95}\text{O}_{3.95}\text{F}_{0.05}$ ( $\text{Mn}_2\text{O}_3 + \text{LiF}$ )	29.4	55.4

space group (a subgroup of  $Fd\bar{3}m$ ), which exhibits tripling of the  $a$  and  $b$  axes.<sup>41</sup> Table IV shows the refined cubic and corresponding orthorhombic lattice parameters for each of the materials. To simplify comparison with the cubic  $Fd\bar{3}m$  space group, the superstructure has been ignored, the orthorhombic parameters being expressed as  $a/3$ ,  $b/3$ , and  $c$ . In laboratory X-ray data the superstructure reflections are not visible, so for these purposes the simplification is not unreasonable. It can be seen that there was a decrease in both cubic and orthorhombic lattice parameters with increasing fluorine con-

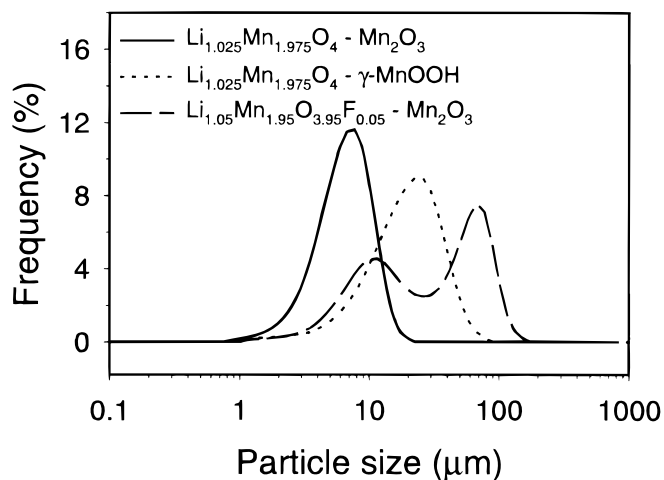


**Figure 7.** Volume distribution of the particle size analysis for high-temperature (HT) synthesized  $\text{Li}_{1.025}\text{Mn}_{1.975}\text{O}_4$  and HT- $\text{Li}_{1.05}\text{Mn}_{1.95}\text{O}_{3.95}\text{F}_{0.05}$ .

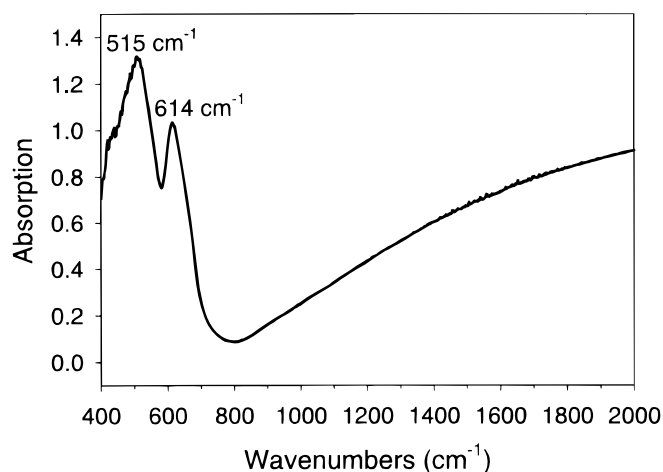


**Figure 8.** FTIR spectrum of HT- $\text{Li}_{1.025}\text{Mn}_{1.975}\text{O}_4$  synthesized using  $\text{LiOH}\cdot\text{H}_2\text{O} + \text{Mn}_2\text{O}_3$ .

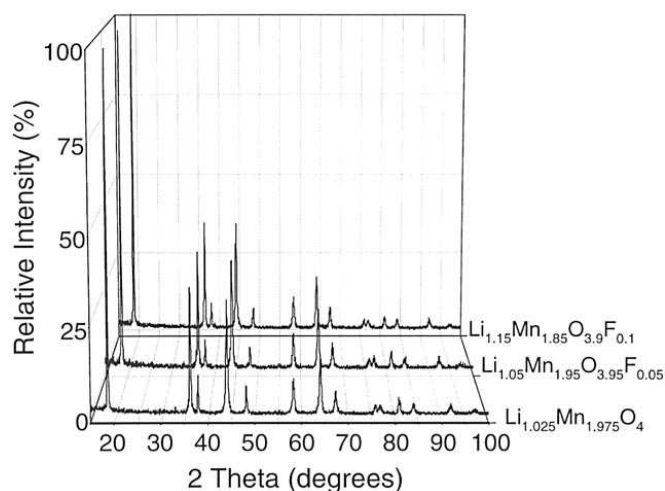


**Figure 9.** Normalized XRD patterns for LT-Li<sub>1.025</sub>Mn<sub>1.975</sub>O<sub>4</sub>, LT-Li<sub>1.05</sub>Mn<sub>1.95</sub>O<sub>3.95</sub>F<sub>0.05</sub>, and LT-Li<sub>1.15</sub>Mn<sub>1.85</sub>O<sub>3.9</sub>F<sub>0.1</sub>.

tent. This would be expected due to the increasing nominal manganese oxidation state of the stoichiometries. The apparent orthorhombic distortion of the materials also decreased slightly with increasing fluorine content, which in this case is equivalent to increasing manganese oxidation state.

The pseudo-cubic *a* parameters for Li<sub>1.025</sub>Mn<sub>1.975</sub>O<sub>4</sub> and Li<sub>1.05</sub>Mn<sub>1.95</sub>O<sub>3.95</sub>F<sub>0.05</sub> corresponded closely to those expected from their nominal average manganese oxidation states. *a* for low-temperature (LT)-Li<sub>1.025</sub>Mn<sub>1.975</sub>O<sub>4</sub> did not differ significantly from that of high-temperature (HT)-Li<sub>1.025</sub>Mn<sub>1.975</sub>O<sub>4</sub> synthesized with Mn<sub>2</sub>O<sub>3</sub>. The lattice parameter for Li<sub>1.15</sub>Mn<sub>1.85</sub>O<sub>3.9</sub>F<sub>0.1</sub> was that expected from an oxidation state of approximately +3.57<sup>42</sup> rather than the nominal +3.65. This could be explained by an incomplete reaction, which was possible given the low synthesis temperature and the difficulties in detecting low levels of secondary phases by laboratory X-ray powder diffraction.

Atomic absorption/emission results for each of the materials are shown in Table V. The Li:Mn ratios were calculated from a fixed manganese value. It can be seen that each of the materials was close to its nominal stoichiometry within error. In no instance was there any detectable lithium loss during processing.

SEM micrographs in Fig. 10a and b show that the LT-Li<sub>1.025</sub>Mn<sub>1.975</sub>O<sub>4</sub> retained the particle size and shape of the  $\gamma$ -MnOOH reactant. The addition of fluorine in this case made little difference to the particle size or shape, as seen in Fig. 10c and d. This was probably due to the lower synthesis temperature. It can be seen that the needle-shaped particles were approximately 1.2  $\mu$ m long by 0.2  $\mu$ m wide. This agrees well with the number distribution of the particle size, seen in Fig. 11, which gave a median of 0.45  $\mu$ m assuming a spherical particle shape. Although the volume distribution is most commonly quoted in literature, it is often useful to compare SEM micrographs with the number distribution. Volume distributions are heavily biased by small numbers of large agglomerates.

**Table IV. Refined pseudo-cubic and “normalized” orthorhombic lattice parameters for the low-temperature synthesized materials.**

Material	<i>Fd</i> $\bar{3}m$ <i>a</i> parameter (Å)	<i>Fddd</i> lattice parameters (Å) <i>a</i> /3, <i>b</i> /3, and <i>c</i>	<i>Fddd</i> <i>c</i> /( <i>a</i> /3)
Li <sub>1.025</sub> Mn <sub>1.975</sub> O <sub>4</sub>	8.2358	8.256, 8.235, 8.218	0.9954
Li <sub>1.05</sub> Mn <sub>1.95</sub> O <sub>3.95</sub> F <sub>0.05</sub>	8.2220	8.242, 8.221, 8.208	0.9959
Li <sub>1.15</sub> Mn <sub>1.85</sub> O <sub>3.9</sub> F <sub>0.1</sub>	8.2118	8.236, 8.201, 8.205	0.9962

**Table V. Atomic absorption analysis results for low-temperature Li<sub>1.025</sub>Mn<sub>1.975</sub>O<sub>4</sub>, Li<sub>1.05</sub>Mn<sub>1.95</sub>O<sub>3.95</sub>F<sub>0.05</sub>, and Li<sub>1.15</sub>Mn<sub>1.85</sub>O<sub>3.9</sub>F<sub>0.1</sub>.**

Material–Nominal stoichiometry	Measured stoichiometry
Li <sub>1.025</sub> Mn <sub>1.975</sub> O <sub>4</sub>	Li <sub>1.04±0.07</sub> Mn <sub>2.00±0.08</sub> O <sub>3.91±0.18</sub> Relative to Mn = 2.0
Li <sub>1.05</sub> Mn <sub>1.95</sub> O <sub>3.95</sub> F <sub>0.05</sub>	Li <sub>1.14±0.09</sub> Mn <sub>1.95±0.09</sub> O <sub>3.93±0.21</sub> F <sub>0.05</sub> Relative to Mn = 1.95 and F = 0.05
Li <sub>1.15</sub> Mn <sub>1.85</sub> O <sub>3.9</sub> F <sub>0.1</sub>	Li <sub>1.28±0.10</sub> Mn <sub>1.85±0.08</sub> O <sub>3.83±0.20</sub> F <sub>0.1</sub> Relative to Mn = 1.85 and F = 0.1

Unusual LiMn<sub>2</sub>O<sub>4</sub> particle morphologies have been reported previously.<sup>7,43</sup> Amundsen *et al.* used self-assembling surfactants in a sol-gel process,<sup>43</sup> while Larcher *et al.* used polyol precursors to produce plate-like particles.<sup>7</sup> The synthetic simplicity of the microwave technique to synthesize such particles contrasts markedly with the intricacies of the two solution-based methods.

Results of Brunauer-Emmett-Teller (BET) surface area analyses are shown in Table VI. The values obtained were lower than one would expect from examining the micrographs in Fig. 10 and are in fact smaller than spinel made from  $\gamma$ -MnOOH in a conventional low-temperature solid-state process.<sup>44</sup> In this case the surface area was dominated by a relatively small number of large particles, as reflected in the volume particle distributions in Table VII. Spinel particles of a small size are generally thought of as vulnerable to manganese dissolution due to their high surface area to volume ratio. The results from the number distribution of the particle sizes suggest that localized manganese dissolution might be a bigger issue than both the volume distribution and BET results suggest. The agglomerates present in the LT-Li<sub>1.025</sub>Mn<sub>1.975</sub>O<sub>4</sub> were loosely bound and could be broken up relatively easily by the application of ultrasonic energy, as demonstrated in Fig. 12.

Infrared spectroscopy should theoretically be able to detect the changes brought about by the fluorine substitution. The presence of fluorine would cause a shift in the Mn-O(F) absorptions brought about by changes in the average bond energies. In these materials the situation is complicated by the simultaneous substitution of Li onto the Mn site, yielding different average Mn oxidation states. The Mn oxidation states within Li<sub>1.025</sub>Mn<sub>1.975</sub>O<sub>4</sub> and Li<sub>1.15</sub>Mn<sub>1.975</sub>O<sub>3.9</sub>F<sub>0.1</sub> are different as evidenced by their pseudo-cubic lattice parameters (8.212 vs. 8.239 Å); therefore, it was useful to see if any shifts in the IR absorptions were detectable.

As seen in Fig. 13, a very slight shift is observed in the band at 614 cm<sup>-1</sup> to a higher energy (630 cm<sup>-1</sup>) in the fluorinated material. With the limitations of FTIR, a shift of this magnitude with an instrument with 4 cm<sup>-1</sup> resolution is not conclusive, however, it is consistent with the higher manganese oxidation state of the fluorinated material. The weak absorption band at approximately 1120 cm<sup>-1</sup> is due to trace amounts of  $\gamma$ -MnOOH, which exhibits a triplet in this region.<sup>36</sup>

This trace presence of  $\gamma$ -MnOOH in the IR, and absence of  $\beta$ -MnO<sub>2</sub> in any of the X-rays, provide clues as to temperature conditions present during low-temperature synthesis. However, the situation is complicated by the large variation in decomposition behavior of  $\gamma$ -MnOOH with oxygen partial pressure.<sup>45</sup> Although the crucibles were not sealed in inert gas, their construction with the porcelain lid may lead to purging of the atmosphere within the crucible from steam driven off the LiOH·H<sub>2</sub>O, leading to uncertainty in the level of available oxygen.

In air,  $\gamma$ -MnOOH decomposes to  $\beta$ -MnO<sub>2</sub> at 300°C, which then decomposes to Mn<sub>2</sub>O<sub>3</sub> at 600°C.<sup>45</sup> However this is known to drop to ~485°C in the presence of LiOH.<sup>46</sup> With a reduced oxygen partial pressure,  $\gamma$ -MnOOH decomposes to Mn<sub>2</sub>O<sub>3</sub> at 300°C as opposed to  $\beta$ -MnO<sub>2</sub>.<sup>45</sup> The microwave absorption characteristics of  $\beta$ -MnO<sub>2</sub> and Mn<sub>2</sub>O<sub>3</sub> differ greatly. If  $\beta$ -MnO<sub>2</sub> was produced then the temperature could have risen to its decomposition temperature due to

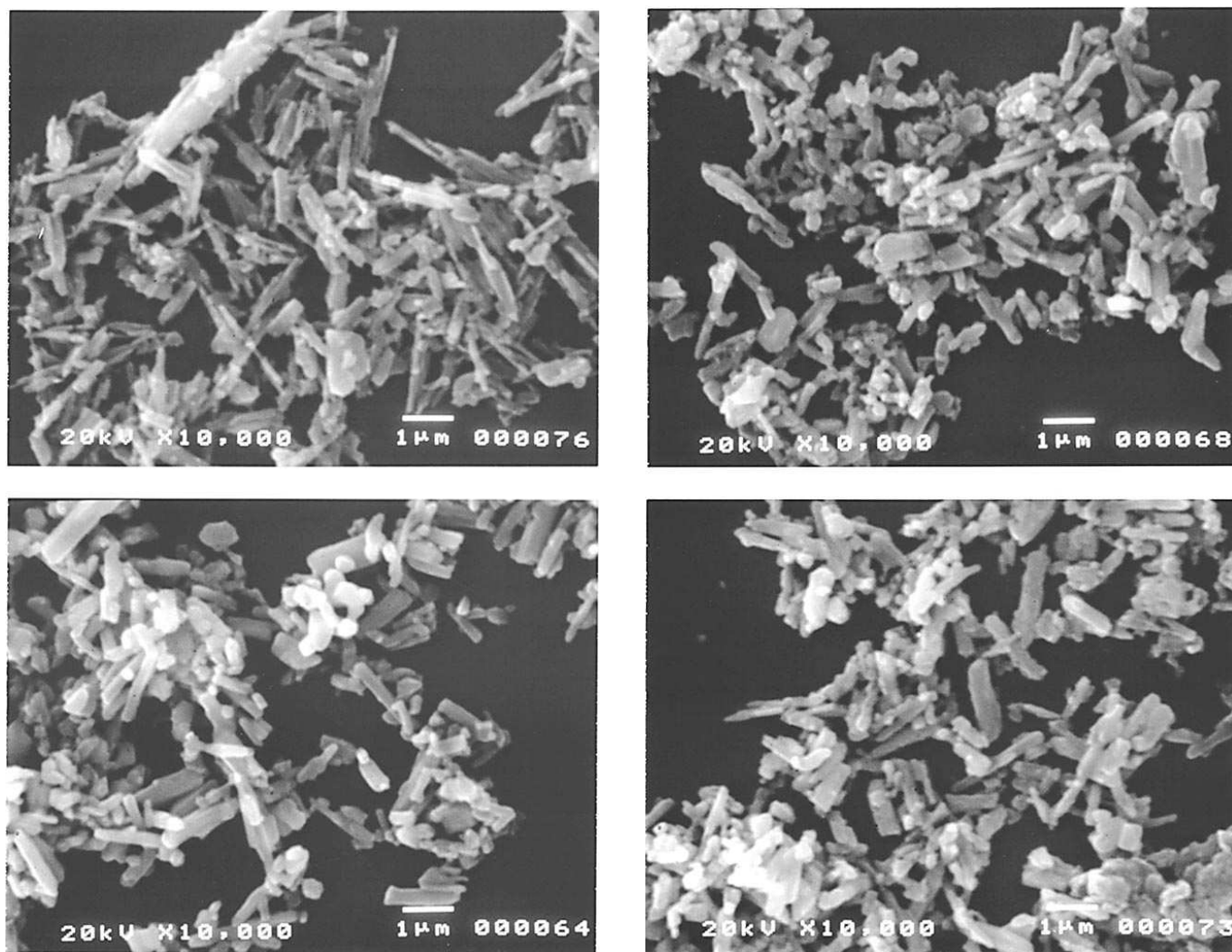


**Figure 10.** SEM micrographs of (a, top left)  $\gamma$ -MnOOH, (b, top right)  $\text{LT-Li}_{1.025}\text{Mn}_{1.975}\text{O}_4$ , (c, bottom left)  $\text{LT-Li}_{1.05}\text{Mn}_{1.95}\text{O}_{3.95}\text{F}_{0.05}$ , and (d, bottom right)  $\text{LT-Li}_{1.15}\text{Mn}_{1.85}\text{O}_{3.9}\text{F}_{0.1}$ .

efficient microwave energy absorption, producing  $\text{Mn}_2\text{O}_3$ .  $\text{Mn}_2\text{O}_3$  is a poor microwave absorber at lower temperatures, so it must rely on

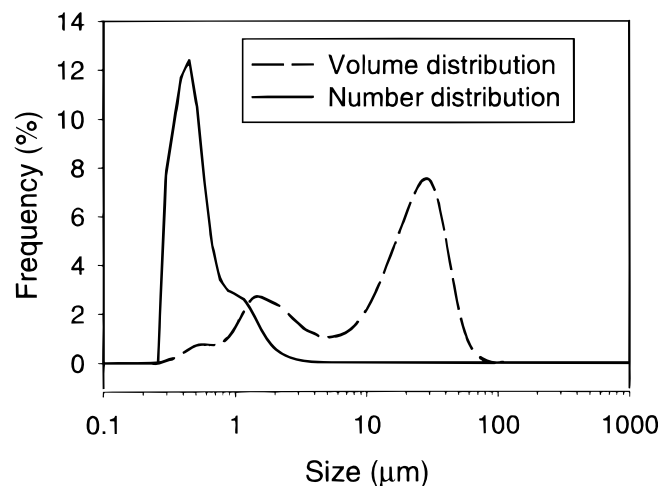


**Figure 11.** Particle size distribution of  $\text{LT-Li}_{1.025}\text{Mn}_{1.975}\text{O}_4$  presented in both volume and number distributions. The distributions were calculated using a spherical particle model and a refractive index of 1.19.

the  $\text{CuO}$  secondary susceptor to provide the necessary energy. The behaviors of  $\text{Mn}_2\text{O}_3$  and  $\text{LiMn}_2\text{O}_4$  in a microwave field at elevated temperatures have never been measured; therefore, it is impossible to say whether they contribute further to the heating provided by  $\text{CuO}$  at higher temperatures. Once again, the possible influence of an electromagnetic field on thermal decomposition temperatures and mechanisms add further uncertainty.<sup>47</sup> Assuming oxygen levels similar to air in the crucible, together with the absence of a visible glow in the  $\text{CuO}$ , one may speculate that the maximum peak temperature reached in the crucible was in the region of  $500^\circ\text{C}$ , although the presence of  $\gamma$ -MnOOH in the IR spectra would suggest that such temperatures could not have endured for a long period.

Figure 14 shows DSC results for (a)  $\text{LT-Li}_{1.15}\text{Mn}_{1.85}\text{O}_{3.9}\text{F}_{0.1}$  and (b)  $\text{LT-Li}_{1.025}\text{Mn}_{1.975}\text{O}_4$ .  $\text{LT-Li}_{1.025}\text{Mn}_{1.975}\text{O}_4$  exhibited a weak endotherm between  $105$  and  $125^\circ\text{C}$ . Given its proximity to  $100^\circ\text{C}$

**Table VI.** BET surface areas of low-temperature synthesized materials.

Material	BET surface area ( $\text{m}^2/\text{g}$ )	% Error
$\text{Li}_{1.025}\text{Mn}_{1.975}\text{O}_4$	2.1	0.2
$\text{Li}_{1.05}\text{Mn}_{1.95}\text{O}_{3.95}\text{F}_{0.05}$	1.7	0.5
$\text{Li}_{1.15}\text{Mn}_{1.85}\text{O}_{3.9}\text{F}_{0.1}$	1.8	0.4

**Table VII. Particle sizes of the low-temperature synthesized materials.**

Material	Mean particle size volume distribution (μm)	Mean particle size number distribution (μm)
Chemetals γ-MnOOH	0.4	0.43
Li <sub>1.025</sub> Mn <sub>1.975</sub> O <sub>4</sub>	14.2	0.51
Li <sub>1.05</sub> Mn <sub>1.95</sub> O <sub>3.95</sub> F <sub>0.05</sub>	12.0	0.50
Li <sub>1.15</sub> Mn <sub>1.85</sub> O <sub>3.9</sub> F <sub>0.1</sub>	14.0	0.52

one would expect that this was due to absorbed water and/or water of crystallization. However, although reproducible for the unfluorinated material, the fluorinated product did not show the same feature. As the fluorinated material had very similar particle size and morphology, one might expect that it would have a similar affinity for the absorption of surface water. The FTIR results suggest that a similar quantity of residual γ-MnOOH remains in both materials. For comparison purposes the DSC curves for (c) the starting γ-MnOOH and (d) a commercial LiMn<sub>2</sub>O<sub>4</sub> material were obtained. The origin of this endotherm is currently unknown.

### Conclusions

Both fluorinated and unfluorinated spinels have been synthesized utilizing microwave radiation as the energy source. Syntheses were successful at both high and low applied powers, the reaction rates being significantly accelerated in all cases. Product particle morphologies varied according to starting materials and synthesis temperature. Interestingly this seems to contradict the findings of Yan *et al.*,<sup>29</sup> who stated that the particle shape and size remain the same as the starting material. This is definitely not the case with γ-MnOOH at high temperature.

Interestingly, material synthesized at low power using γ-MnOOH as the Mn source exhibited needle-shaped particles. Particle sizes were generally small, although grain growth could be accelerated and crystallinity enhanced by the addition of fluorine in the form of LiF. Small particles are normally not regarded as optimal for spinel electrochemical properties, although other cathode materials are more forgiving in this respect. Particle size and shape may be affected through extended heating or the use of mineralizers such as LiF.

Microwave synthesis appears to be a credible option for rapid and energy-efficient synthesis of LiMn<sub>2</sub>O<sub>4</sub>. Together with the use of secondary susceptors where necessary, there is no reason why microwave synthesis could not be extended successfully to other oxide electrode materials.

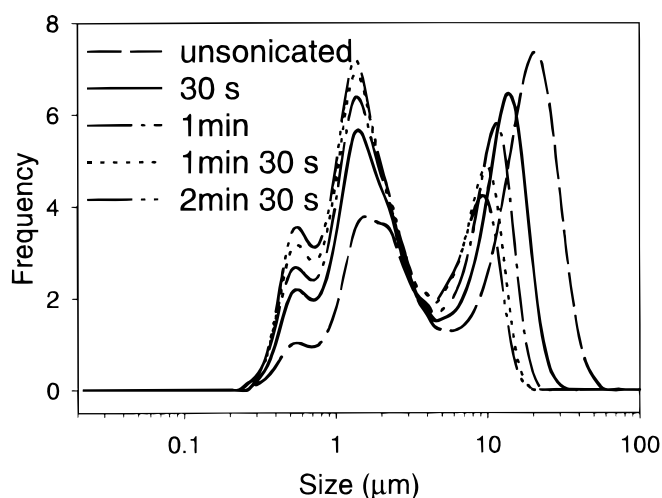


**Figure 12.** Evolution of volume distribution of particle size of LT-Li<sub>1.025</sub>Mn<sub>1.975</sub>O<sub>4</sub> with sonication time.

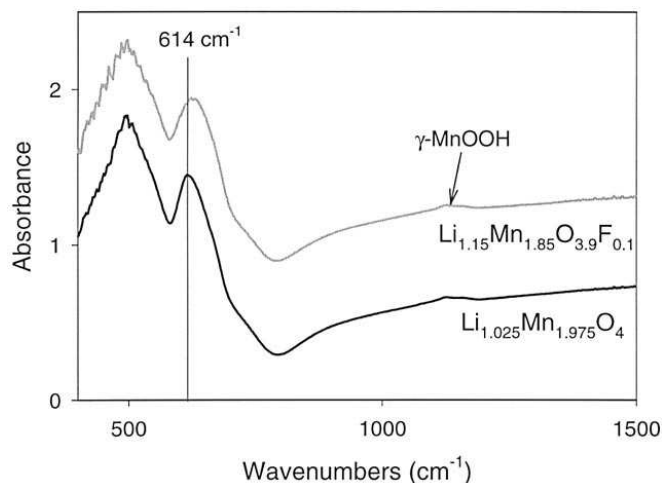


**Figure 13.** FTIR spectra of LT-Li<sub>1.025</sub>Mn<sub>1.975</sub>O<sub>4</sub> and LT-Li<sub>1.15</sub>Mn<sub>1.85</sub>O<sub>3.9</sub>F<sub>0.1</sub>.

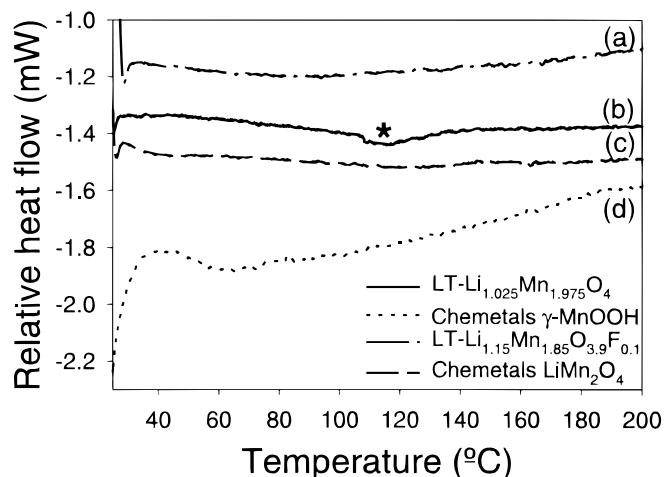


**Figure 14.** DSC curves for (a) LT-Li<sub>1.15</sub>Mn<sub>1.85</sub>O<sub>3.9</sub>F<sub>0.1</sub>, (b) LT-Li<sub>1.025</sub>Mn<sub>1.975</sub>O<sub>4</sub>, (c) Chemetals γ-MnOOH, and (d) Chemetals LiMn<sub>2</sub>O<sub>4</sub>. The asterisk marks an anomalous endotherm exhibited by the LT-Li<sub>1.025</sub>Mn<sub>1.975</sub>O<sub>4</sub>.

### Acknowledgments

The authors would like to acknowledge the assistance of Helen Sleg, Irina Kargina, Steven Argue, Gerry Pleizier, and Floyd Toll with the DSC, FTIR, AA, SEM, and particle size analyses, respectively.

PSW would like to thank the Natural Science and Engineering Research Council of Canada and National Research Council Canada for financial support. The authors also thank Chemetals, Inc., for kindly supplying the γ-MnOOH used in this work.

*The Institute for Chemical Process and Environmental Technology assisted in meeting the publication costs of this article.*

### References

1. P. G. Bruce, *Chem. Commun.*, 1817 (1997).
2. M. M. Thackeray, *Prog. Solid State Chem.*, **25**, 1 (1997).
3. M. M. Thackeray, P. J. Johnson, L. A. de Picciotto, P. G. Bruce, and J. B. Goodenough, *Mater. Res. Bull.*, **19**, 179 (1984).
4. M. M. Thackeray, W. I. F. David, P. G. Bruce, and J. B. Goodenough, *Mater. Res. Bull.*, **18**, 461 (1983).
5. Y. Xia, H. Zhou, and M. Yoshio, *J. Electrochem. Soc.*, **144**, 2593 (1997).
6. P. Endres, B. Fuchs, S. Kemmler-Sack, K. Brandt, G. Faust-Becker, and H.-W. Praas, *Solid State Ionics*, **89**, 221 (1996).
7. D. Larcher, B. Gerand, and J. M. Tarascon, *J. Solid State Electrochem.*, **2**, 137 (1998).
8. A. du Pasquier, A. Blyr, A. Cressent, C. Lenain, G. G. Amatucci, and J. M. Tarascon, *J. Power Sources*, **81-82**, 54 (1999).

9. M. G. Francesconi and C. Greaves, *Supercond. Sci. Technol.*, **10**, A29 (1997).
10. G. G. Amatucci, A. Blyr, C. Schmutz, and J. M. Tarascon, *Prog. Batt. Mater.*, **16**, 1 (1997).
11. G. G. Amatucci and J. M. Tarascon, U.S. Pat. 5,674,645 (1997).
12. Y. Xia, Y. Hideshima, N. Kumada, M. Nagano, and M. Yoshio, *J. Power Sources*, **24**, 24 (1998).
13. G. G. Amatucci, A. Blyr, C. Sigala, P. Alfonse, and J. M. Tarascon, *Solid State Ionics*, **104**, 13 (1997).
14. T. T. Chen, J. E. Dutrizac, K. E. Haque, W. Wyslouzil, and S. Kashyap, *Can. Met. Quart.*, **23**, 349 (1984).
15. B. Swain, *Adv. Mater. Process.*, **134**, 76 (1989).
16. D. R. Baghurst, A. M. Chippendale, and D. M. P. Mingos, *Nature*, **332**, 311 (1988).
17. M. Kato, K. Sakakibara, and Y. Koike, *App. Supercond.*, **5**, 33 (1997).
18. B. Vaidhyanathan, P. Raizada, and K. J. Rao, *J. Mater. Sci. Lett.*, **16**, 2022 (1997).
19. F. Bondioli, A. Bonamartini Corradi, A. M. Ferrari, C. Leonelli, C. Siligardi, T. Manfredini, and N. G. Evans, *Journal of Microwave Power and Electromagnetic Energy*, **33**, 18 (1998).
20. M. A. Janney and H. D. Kimrey, *Ceram. Pow. Sci.*, **1**, 919 (1988).
21. A. Chatterjee, T. Basak, and K. G. Ayappa, *AIChE J.*, **44**, 2302 (1998).
22. P. Boch and N. Lequeux, *Solid State Ionics*, **101**, 1229 (1997).
23. J. H. Booske, R. F. Cooper, and S. A. Freeman, *Mater. Res. Innov.*, **1**, 77 (1997).
24. D. R. Baghurst and D. M. P. Mingos, in *Microwave-Assisted Chemistry. Fundamentals, Sample Preparations, and Applications*, p. 523, American Chemical Society, Washington, DC (1997).
25. H. Yan, X. Huang, H. Li, and L. Chen, *Solid State Ionics*, **113**, 11 (1998).
26. H. Yan, X. Huang, Z. Lu, H. Huang, R. Xue, and L. Chen, *J. Power Sources*, **68**, 530 (1997).
27. M. Y. Saidi, U.S. Pat. 5,770,018 (1998).
28. K. J. Rao, B. Vaidhyanathan, M. Ganguli, and P. A. Ramakrishnan, *Chem. Mater.*, **11**, 882 (1999).
29. H. Yan, X. Huang, and L. Chen, *J. Power Sources*, **81-82**, 647 (1999).
30. Y. Xu and X. Xiao, *J. Mater. Res.*, **10**, 334 (1995).
31. Z. Xie, X. Fan, and Y. Huang, *J. Mater. Res.*, **13**, 3417 (1998).
32. W. Kraus and G. Nolze, *J. Appl. Crystallogr.*, **29**, 301 (1996).
33. A. C. Larson and R. B. Von Dreele, General Structure Analysis System, LAUR 86-748, Los Alamos National Laboratory, Los Alamos, NM (1994).
34. Y. Gao and J. R. Dahn, *J. Electrochem. Soc.*, **143**, 1783 (1996).
35. J. M. Tarascon, W. R. McKinnon, F. Coowar, T. N. Bowmer, G. G. Amatucci, and D. Guyomard, *J. Electrochem. Soc.*, **141**, 1421 (1994).
36. T. Kohler, T. Armbruster, and E. Libowitzky, *J. Solid State Chem.*, **133**, 486 (1997).
37. P. J. Hirst, A. Drake, M. Rand, and J. S. Abell, *Physica C*, **235-240**, 371 (1994).
38. G. E. Bacon, *Neutron Scattering in Chemistry*, pp. 177-178, Butterworth and Company, London (1977).
39. B. Ammundsen, G. R. Burns, M. S. Islam, H. Kanoh, and J. Roziere, *J. Phys. Chem. B*, **103**, 5175 (1999).
40. L. Schütte, G. Colmann, and B. Reuter, *J. Solid State Chem.*, **27**, 227 (1979).
41. G. Rousse, C. Masquelier, J. Rodríguez-Carvajal, and M. Hervieu, *Electrochem. Solid-State Lett.*, **2**, 6 (1999).
42. G. G. Amatucci, C. Schmutz, A. Blyr, C. Sigala, A. S. Gozdz, D. Larcher, and J. M. Tarascon, *J. Power Sources*, **69**, 11 (1997).
43. B. Ammundsen, D. J. Jones, J. Roziere, and G. R. Burns, *Chem. Mater.*, **9**, 3236 (1997).
44. Y. Xia and M. Yoshio, *J. Power Sources*, **57**, 125 (1995).
45. C. González, J. I. Gutiérrez, J. R. González-Velasco, A. Cid, A. Arranz, and J. F. Arranz, *J. Thermal Anal.*, **47**, 93 (1996).
46. I. Kargina, Unpublished TGA results, ICPET, National Research Council Canada (1997).
47. E. M. Zingel, *Thermochim. Acta*, **198**, 191 (1991).